Astron. Astrophys. 253, 269–276 (1992)

ASTRONOMY AND ASTROPHYSICS

Dynamics of flaring loops

II. Flare evolution in the density-temperature diagram

J. Jakimiec [1], B. Sylwester [2], J. Sylwester [2], S. Serio [3,4], G. Peres [5], and F. Reale [4]

[1] Institute of Astronomy, Wrocław University, PL-51-622 Wrocław, Poland
[2] Space Research Centre, Polish Academy of Sciences, PL-51-622 Wrocław, Poland
[3] Istituto di Astronomia and Osservatorio Astronomico, I-90134 Palermo, Italy
[4] Istituto per le Applicazioni Interdisciplinarie della Fisica, CNR, I-90134 Palermo, Italy
[5] Osservatorio Astrofisico, I-95125 Catania, Italy

Received May 28, accepted July 16, 1991

Abstract. In the present paper the evolution of basic thermodynamic parameters of a single flaring solar loop has been investigated in terms of density-temperature (N–T) diagram. A grid of hydrodynamic models has been calculated for this purpose using the Palermo-Harvard code. The calculated models differ in their initial conditions and the form of the energy input i.e. the heating rate value, the heating duration, the assumed time profile.

We have considered the consequences of variation of these model parameters on the evolutionary paths in the density-temperature diagrams. We show that, over a substantial duration, the decay occurs along a $T \propto N^2$ trajectory when the impulsive flare heating function is switched-off abruptly. The results obtained in this paper can be very useful as diagnostics of the flare heating process based on soft X-ray observations.

Key words: hydrodynamics – Sun, corona – Sun, flares

1. Introduction

In a previous paper (Serio et al. 1991; henceforth Paper I) we have investigated the decay of simple solar flare loops under simplifying assumptions, and demonstrated that the decay proceeds through a "linear phase" during which the entropy per particle at the top of the loop decays linear with a rate depending only on the loop length and the initial temperature. We have also shown that, during the linear phase, the decay of temperature and density at the top of the loop is approximately exponential, and found empirical relations among the respective decay times and the entropy decay rate. We have noted that the relationship between the density decay time and the temperature decay time forces a $T \propto N^2$ relationship during the linear phase of a flare loop evolution in solar environment.

In the present paper we want to investigate the evolution of basic thermodynamic parameters (density and temperature) of the flare plasma and its diagnostic value.

Send offprint requests to: B. Sylwester

We have computed the value of these thermodynamic variables for a grid of hydrodynamic flare loop models under a number of different assumptions. We have used the Palermo-Harvard code (Peres et al. 1982; Peres & Serio 1984), which solves the one-dimensional hydrodynamic equations of mass, momentum and energy conservation for a solar plasma confined in a semicircular arch of constant cross section. The plasma is assumed to be in ionization equilibrium. The equations take into account effects of gravity, viscosity, Spitzer thermal conduction, and radiation losses from an optically thin plasma. A background uniform heating term, $(E_H)_0$, (necessary to maintain the loop in thermal equilibrium during the non-flaring phase) is provided, in addition to a flare heating term, $E_H(t)$, as discussed below. The loop is assumed symmetric at its apex, and therefore with velocity and spatial derivatives of temperature and density equal to zero at the loop top. The temperature at the loop base, located at the temperature minimum (i.e. 4400 K) is maintained constant. The steady-state initial atmosphere is computed as in Serio et al. (1981) for the coronal part, and matched to an appropriate Vernazza et al. (1980) chromospheric model at $T \approx 2\ 10^4$ K.

Four groups of models, differing in the time profile of the heating function were analyzed (see Table 1):

(1) With instant switch-on and -off, constant in time heating, operating for 50, 100, 180, 300 and 600 s.

(2) With various values of the flare heating rate operating for 180 s, and instant switch-on and -off.

(3) With the heating function of triangular shape, having a linear rise and/or fall.

(4) With instant switch-on, constant in time heating, operating for 180 s and 300 s followed by exponential decay characterized by e-folding times τ of 60, 300 or 1200 s.

We have analyzed also a special group of models already discussed in Paper I. These models investigate only a decay (cooling) phase of flaring loops which are assumed to be in a high-temperature steady-state at the beginning of the model calculations.

In this paper we present an analysis of the flare evolution in terms of density-temperature (N–T) diagrams. Jakimiec et al. (1986, 1987) have shown such that diagrams are very useful in understanding the time evolution of the flare energy release. The (N–T) diagram represents a history of variations of T_{top} vs N_{top}

Table 1. Characteristics of the flare models used in this work

(1) Different duration of the heating

Initial conditions in the steady-state pre-flare loop:
Semi-length $L = 20$ Mm
Top temperature $T_{top} = 3.2$ MK
Top density $N_{top} = 6.12\ 10^9$ cm^{-3}
Background heating rate $(E_H)_0 = 1.35\ 10^{-2}$ ergs cm^{-3} s^{-1}
Flare heating rate $E_H = 10$ ergs cm^{-3} s^{-1}
applied at $t = 0$, lasting for 50, 100, 180, 300 and 600 s, with abrupt switch-off to the pre-flare value.

(2) Different value of the heating rate

Initial conditions in the loop as in *(1)*.
Flare heating rate of log $E_H = 0.0, 0.2, 0.4, 0.6, 0.8$ and 1.0 applied at $t = 0$ s, lasting for 180 s with abrupt switch-on and -off.

(3) Different time profile of the heating rate

Initial conditions in the loops:
Semi-lengths $L = 50$ Mm (LNL), and 10 Mm (SHL)
Top temperature $T_{top} = 3.0$ MK
Top densities $N_{top} = 1.8\ 10^9$ and $1.2\ 10^{10}$ cm^{-3}
Background heating rates $(E_H)_0 = 1.55\ 10^{-3}$ and $4.83\ 10^{-2}$ ergs cm^{-3} s^{-1}
Maximum flare heating rate $E_H = 10$ ergs cm^{-3} s^{-1} reached at $t = 50$ s. Heating time profile of triangular symmetric shape. Total duration of flare heating 100 s.
Initial conditions in the loop as in *(1)*.
Maximum flare heating rate $E_H = 10$ ergs cm^{-3} s^{-1}
(a) reached at $t = 0$ s. Linear decrease of the heating rate to the pre-flare value at 200 s (DOWN).
(b) reached at $t = 200$ s. Linear rise of the heating rate with an abrupt switch-off of the heating to pre-flare value afterwards (UP).

(4) Different decay of the heating

Initial conditions in the loop as in *(1)*.
Flare heating rate $E_H = 10$ ergs cm^{-3} s^{-1}
applied at $t = 0$, duration 180 s and 300 s, decreasing with e-folding time $\tau = 60$, 300, and 1200 s to pre-flare value.

plotted in logarithmic sclaes, where T_{top} and N_{top} are the electron temperature and density of the plasma at the top of a flaring loop. Usually T_{top} is the maximum plasma temperature, at least in the cases when the flare heatings is located somewhere near the top of the loop. The values of T_{top} and N_{top} are taken directly from results of the hydrodynamic modelling.

In the next section we present the $(N–T)$ diagram concept and point out advantages of using it in the analysis of the flare evolution. In Sect. 3 the $(N–T)$ diagrams for the decay phase models of Paper I are presented, together with diagrams for a set of models with a complete cycling of the flare heating from zero its peak value and zero again with an abrupt switch-off (cf. the first, second and third group of models from Table 1). In Sect. 4 we discuss the evolution of flares along the quasi-steady-state (QSS) trajectory, i.e. the trajectory implied by the RTV scaling law. Section 5 is devoted to a summary and conclusions.

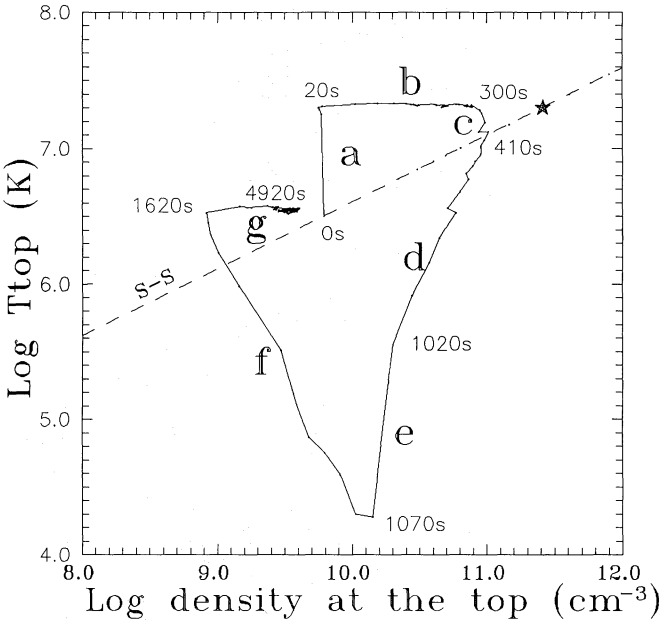

Fig. 1. The density-temperature diagram for plasma located at the top of a loop. The evolutionary path corresponds to the model in which a constant flare heating (switched-on abruptly at $t = 0$) operates for 300 s with an abrupt switch-off to the pre-flare value. Individual phases of the evolution are denoted by letters and described in the text. The dashed line $(S–S)$ in this and all the other figures, represents the relation between the plotted parameters for steady-state conditions (RTV scaling law). The numbers indicate the time elapsed since the start of flare heating

2. Flare evolution in the density-temperature diagram

A typical example of a flare evolutionary path in an $(N–T)$ diagram is presented in Fig. 1. The dashed line in the figure represents the steady-state $(S–S)$ relation (according to the so-called scaling law RTV of Rosner et al. 1978). In the present paper the scaling law is taken in the form:

$$T_{top}^2 = CN_{top}L, \tag{1}$$

where T_{top}, N_{top} are the temperature and density of the plasma at the top of the loop and C is a constant (cf. Jakimiec et al. 1986). The slope of this line is $\xi_{S-S} = 0.5$. The continuous line in the figure represents the variation of T_{top} and N_{top} resulting from calculations of the hydrodynamic flare model (for details of the model see Table 1), where the duration of the heating has been chosen as 300 s. The numbers indicated in the figure denote the time passed from the start of the heating. The letters denote several characteristic phases of the flare evolution:

a *(0 s–20 s):* The flare heating starts from the $S–S$ initial conditions at time $t = 0$ s. After a sudden start of the energy release into the loop, the temperature T_{top} rises very quickly (in a time less than 20 s), immediately adjusting to its maximum value which is determined by the balance between the heating rate E_H and the conductive losses.

b *(20 s–300 s):* Under constant heating, T_{top} does not change substantially and the plasma density, N_{top}, slowly increases. The occurrence of phases **a** and **b** is a natural consequence of the perturbation of initial steady-state conditions. The strong release

of energy cannot be immediately irradiated (coronal plasma is not dense enough) and therefore the plasma temperature increases. This, in turn, leads to an increase of the conductive flux along the loop. The chromospheric plasma at the loop base is heated to high temperatures, expands and violently flows up into the loop i.e. so-called chromospheric evaporation occurs. The evolutionary trajectory runs horizontally towards the S–S line. Under a sufficiently long-lasting constant heating, the S–S conditions would be reached (the asterisk in Fig. 1).

c *(300 s–410 s):* At the moment when the flare heating is suddenly switched-off (at 300 s in the case shown in the figure) a decrease of T_{top} begins. This cooling of the plasma is due to conductive and radiative losses. A delay in reaching the maximum density is seen which is due to the inertia of the evaporated, upward-moving chromospheric plasma, being in motion at the moment of the energy switch-off. Later on, the plasma density decreases as a consequence of the gravitational fall-down. At $t \approx 410$ s, the evolutionary path crosses the steady-state (S–S) line.

d *(410 s–1020 s):* A systematic cooling (due to conductive and radiative losses) and a density decrease take place. The decrease of T_{top} during this phase occurs with a mean rate of $2\ 10^4$ K s^{-1}. A significant part of the thermal energy of the plasma confined in the loop is carried away by the enthalpy flux of the plasma outflowing through the foot points. When T_{top} drops to the pre-flare value ($t \approx 820$ s) the electron density is still much higher than the pre-flare value. Later on, a further cooling causes a further decrease of T_{top} significantly below its initial value.

e *(1020 s–1070 s):* Due to unbalanced large radiative losses the plasma at the loop top becomes thermally unstable (the temperature drops extremely fast with only a small change of the density). A small background heating rate $(E_H)_0$ necessary to maintain the initial steady-state is not able to prevent possible formation of an Hα post-flare loop.

f *(1070 s–1620 s):* During this phase a slow increase of the temperature occurs due to the presence of the continuous background heating $(E_H)_0$. However, N_{top} decreases further as the effect of persistent plasma outflow and after $t = 1170$ s the density becomes lower than in the pre-flare S–S conditions. At some moment the evolutionary path crosses the S–S line again.

g *(1620 s–4920 s):* At the beginning of this phase T_{top} reaches a value close to the pre-flare one. This value is determined by the rate of background heating. N_{top} increases again as the result of slow chromospheric evaporation. If the calculations would be continued for a sufficiently long time the starting values of T_{top} and N_{top} would be restored. Phase **g** resembles phase **b**, but at a temperature level determined by the value of the background heating rate $(E_H)_0$.

3. N–T diagrams for other calculated models

We begin this section with a discussion of the (N–T) diagrams for the family of the decay phase models considered in Paper I. The diagrams are shown in Fig. 2. These models represent a specific but instructive class. In all of them steady-state initial conditions are assumed. According to the high rate of energy deposition, the initial plasma temperature and the density are relatively high.

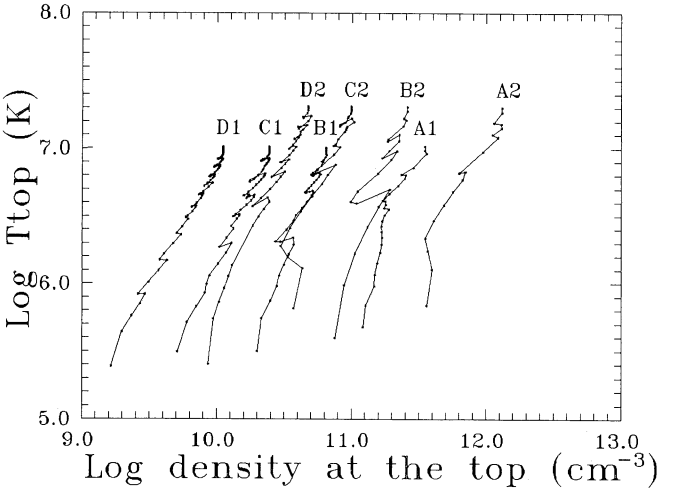

Fig. 2. The density-temperature diagram for the decay phase models (SS-OFF). The letters A, B, C and D in the figure correspond to semi-lengths of 5, 20, 50 and 100 Mm, respectively, and the numbers 1 and 2 represent the initial maximum temperature in units of 10 MK. (This notation is according to Table 1 of Paper I.)

After switch-off of the heating the cooling phase occurs. In the following analysis we shall refer to these models as SS-OFF for brevity. The following initial temperatures at the top, T_{top}, and loop semilengths, L, have been selected in the hydrodynamic calculations: $T_{top} = 10$ and 20 MK, $L = 5$, 20, 50, and 100 Mm (cf. Table 1 of Paper I). It is seen from Fig. 2 that for the SS-OFF models a characteristic pattern of the evolution occurs. The mean slope of all evolutionary trajectories during a relatively long period of the decay is similar, being independent of the loop semilength and the initial temperature. The average slope for all the models is: $\xi = \mathrm{d}(\log T_{top})/\mathrm{d}(\log N_{top}) = 1.96 \pm 0.17$. As noted in Paper I, this is a consequence of the exponential decay of the top temperature occuring with a time constant twice as fast as the exponential decay of density.

In the subsequent paper (Paper III), we shall compare the (N–T) diagrams obtained from the model calculations with the empirical diagrams constructed from soft X-ray observations.

The densities and temperatures derived from analysis of the soft X-ray data represent, in most cases, the mean values, averaged over a substantial portion of the hot flare plasma, since the present X-ray observations have insufficient spatial resolution. Therefore they do not correspond precisely to the conditions at the loop top. Such averaging may affect the trajectories in the (N–T) diagrams. To check the role of such an effect we have examined the evolution of plasma in the (N–T) diagram not only for the loop top, but also for several other positions along the loop length. The following distances from the loop top have been selected: $\Delta s = 0.47$, 0.8, and 0.9 L. As an example of the results, we show in Fig. 3 the diagrams for the D2 model from Paper I. It is seen that individual evolutionary paths for points located at different positions along the loop have practically the same slope, ξ, i.e. the slope determined for the loop top is appropriate for the *entire* flaring loop. This indicates that the observational averaging of plasma parameters over a considerable part of the loop volume (when they are determined from X-ray observations) could result in some displacement of the evolutionary path in the (N–T) diagram, but the characteristic slope should be preserved. We have performed a similar analysis for several other loop models corre-

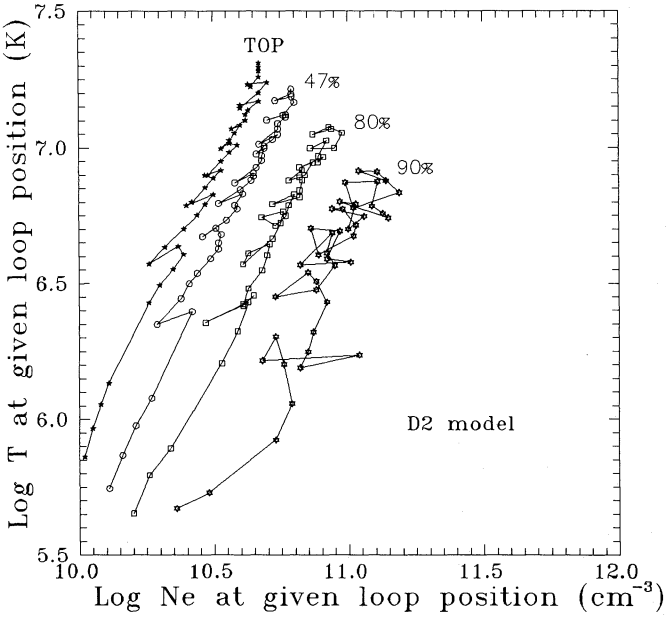

Fig. 3. The density-temperature diagram for the plasma located at selected positions along the loop, for D2 model from Paper I. Numbers denote the distance from the loop top

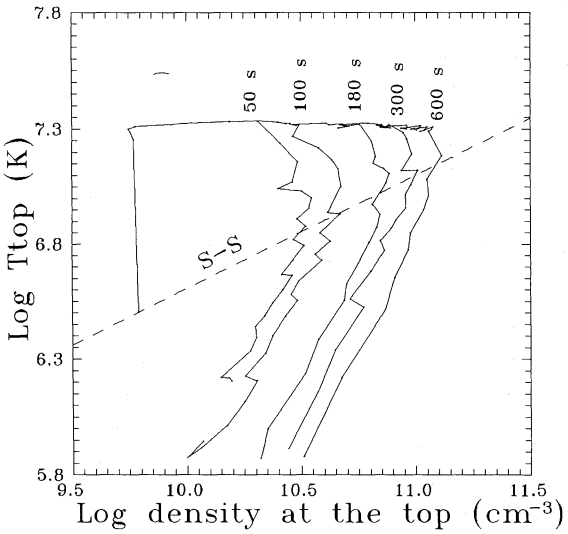

Fig. 4. The density-temperature diagrams for a grid of models characterized by various flare heating phase durations (Δt = 50, 100, 180, 300 and 600 s)

sponding to different initial conditions and the results fully confirm the above conclusion.

To ascertain how the above results can be extended to the case in which the initial state is not steady, but rather a dynamic one, we proceed to a presentation and discussion of the evolutionary paths in (N–T) diagram for three groups of flare models described in Table 1.

In Fig. 4 (analogous to Fig. 1) the evolutionary paths (**a**, **b**, **c**, and **d** phases) for the models with various durations Δt of the flare energy release are presented (the first group from Table 1); Δt = 50, 100, 180, 300, and 600 s have been taken in the calculations. Let us note that $\Delta t = \Delta t_a + \Delta t_b$, ($\Delta t_a$, Δt_b being the durations of phases **a** and **b** respectively) and for most of our cases $\Delta t \approx \Delta t_b$, since Δt_a is short ($\approx$ 20 s for the models shown in Fig. 4).

Table 2. Slopes of the **d**-phase evolutionary paths for the first group of models from Table 1

Δt [s]	ξ	σ
50	1.80	0.11
100	1.86	0.09
180	1.99	0.08
300	2.12	0.07
600	2.11	0.10

One of the natural properties of flare evolution, which is clearly seen in Fig. 4 is the dependence of N_{top} on the duration Δt of the heating. The longer is the duration, the higher is the maximum density achieved.

Another property, which is clearly seen, is that the slopes of the evolutionary paths during the **d**-phase are similar. The values of the slope ξ for the individual evolutionary paths are given in Table 2, together with their estimated standard deviations σ. Values of the slope ξ for the **d**-phase of individual models in this and the other cases considered in the present paper have been calculated by means of fitting a straight line to the coronal part of data points ($T \geqq 1.5$ MK).

A weak dependence of the slope ξ on the duration Δt of the heating is suggested by the values from Table 2. The average value of the **d**-phase slope for all models in Fig. 4 amounts to $\xi = 1.98 \pm 0.15$.

It is worth stressing that the last value is close to that obtained for the SS-OFF models. It is not accidental, if we remember that both the SS-OFF models and **d**-phases of the models shown in Fig. 4 correspond to the decay phase of a flare when the heating is abruptly terminated (the **d**-phase begins when the evolutionary path just crossed the S–S line). Let us also point out that the SS-OFF evolution is actually the **d**-phase for the cases when the flare heating operates so long that the flare reaches the steady-state line *before* the abrupt termination of the heating occurs (see the asterisk in Fig. 1).

In Fig. 5 evolutionary paths are presented for loops (L = 20 Mm), for which various values of the flare heating rate have been adopted (the second group from Table 1). The heating operated for Δt = 180 s for all the cases. The following values of the heating rate were taken $\log E_H$ = 0.0, 0.2, 0.4, 0.6, 0.8 and 1.0. As was shown by Jakimiec et al. (1986) the plasma temperature during the **b**-phase quickly assumes values corresponding to those of the steady-state with the same heating rate. In addition, a dependence of the duration of the **a**-phase on the level of the flare heating can be noticed from Fig. 5. For higher values of E_H the temperature of plasma at the top adjusts very quickly ($\Delta t \leqq 20$ s) to the actual rate of heating, but for lower E_H, it takes longer, as much as 80 s for $E_H = 1\,\mathrm{erg\,cm^{-3}\,s^{-1}}$ case. Consequently, the **b**-phase lasts longer for the former cases and shorter for the latter ones. For the **d**-phases seen in Fig. 5, the slopes ξ are similar to those shown in Table 2.

The above analysis demonstrates that for the **d**-phase of flares we have a characteristic slope ξ in the (N–T) diagram which appears to be $\xi \approx 2$. This ξ value does not strongly depend on the flaring loop parameters such as L – the loop semi-length, T_b – the

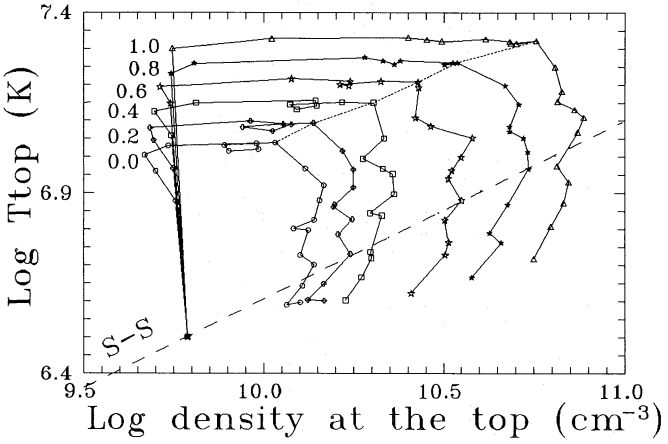

Fig. 5. The density-temperature diagrams for a grid of models for a loop of semi-length 20 Mm. The plasma was heated for 180 s with various heating rates: $\log E_H = 0.0$, 0.2, 0.4, 0.6, 0.8 and 1.0 (abrupt switch-on and -off of the flare heating). The calculations were terminated at $t = 600$ s for all models. The dotted line connects points corresponding to the end of the heating phase (180 s)

temperature during the **b**-phase, and Δt – the heating duration. Moreover, it does not depend on the time-variations of the flare heating function, $E_H(t)$, during the phases **a** and **b** as will be shown below.

In order to investigate this last question we have analyzed the evolutionary paths in the $(N–T)$ diagram for models with various time profiles of the heating function, $E_H(t)$, (the third group of models from Table 1). Appropriate hydrodynamic calculations have been performed for various triangular shapes of $E_H(t)$ by Pallavicini et al. (1983), (see Figs. 12 and 14 in their Paper).

At first, the loop semi-length has been set as 20 Mm and the flare heating duration as 200 s. Two models have been analyzed. In the UP-model the flare heating grows linearly from $E_H = 0$ at $t = 0$ s to its maximum value $E_H = 10$ ergs cm^{-3} s^{-1} at $t = 200$ s followed by an abrupt switch-off. In the DOWN-model the switch-on of the flare heating is abrupt ($E_H = 10$ ergs cm^{-3} s^{-1} at $t = 0$ s) and then it decreases linearly during 200 s (i.e. $E_H = 0$ at $t = 200$ s). The $(N–T)$ diagrams for these two shapes of the heating function together with the evolutionary path for a corresponding SS-OFF model (B1), are shown in Fig. 6. The slope ξ during the **d**-phase is similar for the UP and DOWN models and amounts to 1.82 ± 0.08 and 1.80 ± 0.06, respectively.

The other two examples considered correspond to the hydrodynamic calculations in which the heating rate rises and falls gradually. In these cases the flare heating reaches a peak rate of $E_H = 10$ ergs cm^{-3} s^{-1} at the time $t = 50$ s and a total heating duration of 100 s is assumed. The flare heating has been applied to two different loop structures: one of semi-length $L = 50$ Mm, (the LNL-model) and the other with $L = 10$ Mm, (the SHL-model). The initial temperature at the top has been taken to be the same ($T_{top} \approx 3$ MK) in both cases, which means that the base pressure is different in each of the cases. The $(N–T)$ diagrams for these models are presented in Figs. 7a and 7b. The dashed lines in the figures correspond to the $S–S$ models with the two different loop semi-lengths.

The following values of the slope ξ for the **d**-phase have been obtained: $\xi \approx 1.56 \pm 0.08$ for the LNL model and $\xi \approx 1.72 \pm 0.13$ for the SHL model. These values and the values of ξ from Table 2 suggest the presence of some dependence of ξ on the maximum density, N_{max}, which is reached during the **c**-phase of the model evolution. The low ξ-values correspond to small values of N_{max}, i.e. to the cases when the flaring loop has been poorly filled up with the matter during the **b**-phases of the flare. The LNL model is an example of such a case. This model represents a relatively long loop with a low heating rate ($\bar{E}_H = 5$ ergs cm^{-3} s^{-1}), for which the **b**-phase is rather short ($\Delta t_b \approx 50$ s), while the **a**-phase is prolonged. As a consequence the loop is poorly filled up with plasma and the maximum density, N_{max}, reached during the **c**-phase is very low. Let us note that such cases (low ξ- and low N_{max}-values) can be easily recognized in X-ray flare observations, since these will be flares with short **b**-phases and small emission measure values, $N_{max}^2 V$, i.e. these will be very faint flares.

Now let us compare the evolution of the flaring loops shown in Figs. 1 and 7b (the SHL model). It is clearly seen that the **e**-phase (a quick radiative cooling) is absent in Fig. 7b. This is due

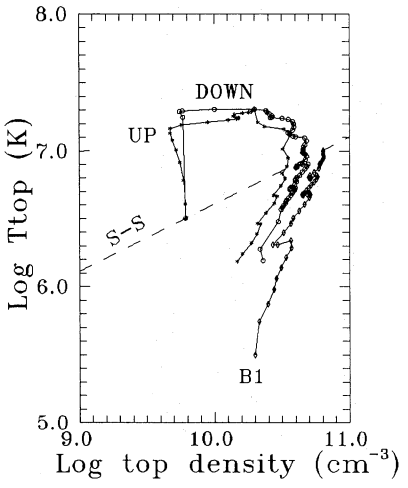

Fig. 6. The density-temperature diagram for UP and DOWN models (see Table 1 for details). For comparison, the corresponding SS-OFF model is shown

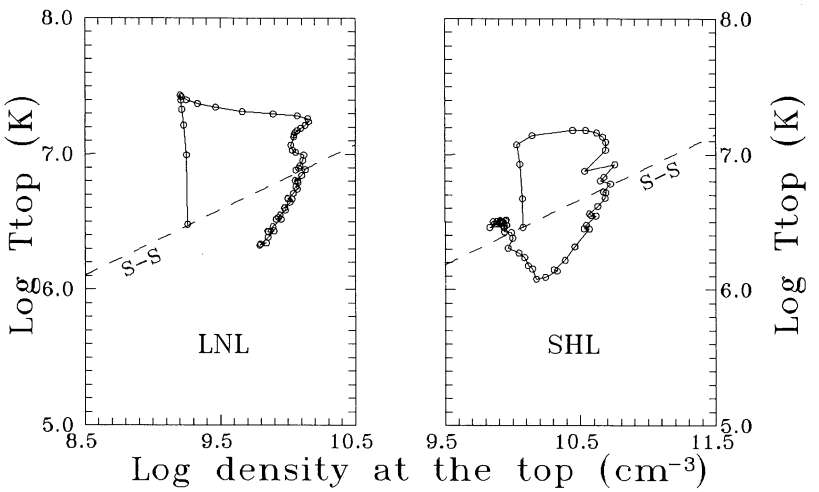

Fig. 7a and b. The density-temperature diagram for LNL (**a**) and SHL (**b**) models. See Table 1 for details of the models

to rather large value of the background (non-flare) heating rate, $(E_H)_0$, in the case of the SHL model. The initial, pre-flare steady-state temperatures are similar for both the cases (see Table 1), but they differ significantly in their $(E_H)_0$ values. This is a consequence of the fact that for the steady-state conditions E_H strongly depends on the loop semilength L (cf. Jakimiec et al. 1986),

$$E_H = 1.0\ 10^{-6}\ T_{top}^{3.5}\ L^{-2}. \quad (2)$$

Since the L-values are 10 and 20 Mm for the SHL model and for the model shown in Fig. 1, respectively, the background heating rate is about 4 times higher for the former than for the latter case (cf. Table 1 for exact values). The increased background heating $(E_H)_0$ in the SHL model takes early control of the loop evolution and the temperature T_{top} does not decrease below 10^6 K. The thermal instability, which occurs when $T \lesssim 5\ 10^5$ K, does not develop and so the phase **e** does not occur (cf. Fig. 7b).

Fisher & Hawley (1990) pointed out that it is helpful to use global quantities in the analysis of flare loop evolution. It turned out that the total number of electrons in the high temperature portion of the loop belongs to this class of global parameters. We have introduced N_{tot} for a loop of unit cross-section and the semi-length L according to the following formula:

$$N_{tot} = \int_{l(T=0.5\,MK)}^{L} N_e\, dl = \bar{N} L, \quad (3)$$

where $\bar{N}$ is the mean electron density in the loop. Using the variable N_{tot} instead of N_{top}, modified diagnostic diagrams shown in Fig. 8 can be constructed. These diagrams present the evolution for the SS-OFF models, which were already discussed (cf. Fig. 2). Inspection of Fig. 8 allows to make the following remarks:

(1) The models exhibit a behaviour very similar to that seen in Fig. 2. The portion of the evolutionary path with a constant slope ($\xi \approx$ const.) is well defined and the corresponding ξ-values are practically the same as in the case of Fig. 2.

(2) The structure of the diagram becomes simpler than that of Fig. 2; the evolutionary paths are clumped now into two separate groups corresponding to different initial temperatures ($T_0 = 10$ MK and 20 MK respectively). The clumping happens since for the steady-state models the scaling law, cf. Eq. (1), expressed in terms of the new variable (N_{tot}) does not contain a dependence on the loop semi-length L: $T_{top}^2 = C\bar{N}L = C N_{tot}$.

(3) By using the integrated density N_{tot} the fluctuations in the evolutionary paths are significantly reduced (compare Figs. 8 and 2). This is of great importance when we determine and compare the values of the slope ξ in the diagrams.

4. Quasi-steady-state flare evolution

In previous papers (Jakimiec et al. 1986, 1987), empirical (N–T) diagrams have been constructed using observations of flare X-ray radiation. In those papers it has been found that during the decay phase of big flares, the evolutionary path often follows a line with slope $\xi \approx 0.5$. This has been interpreted as flare evolution along the line of steady-state models (cf. S–S line in Fig. 1 and the following Figures) when the decay of the heating function $E_H(t)$ is sufficiently slow. Such a pattern of flare evolution has been called quasi-steady-state (QSS) evolution. To examine the QSS evolution more carefully we have performed a suitable set of model calculations concentrating our attention on two problems.

(1) First, we have investigated how slow the decrease of the heating E_H should be in order that the QSS-evolution occurs. To check this, we start with a hot steady-state model of the loop ($L = 20$ Mm, $E_H = a = 8.2$ ergs cm^{-3} s^{-1}) and we allow E_H to decrease exponentially:

$$E_H = a \exp(-t/\tau) \quad \text{for} \quad t > 0. \quad (4)$$

Calculations have been carried out for the following values of the e-folding decay time τ: 300, 600, and 1200 s, and the resulting (N–T) diagrams are shown in Fig. 9. It is seen that for $\tau = 300$ s the evolutionary path initially somewhat deviates from the QSS-branch (S–S line in Fig. 9) but, later on, it runs almost parallel to this branch. For the latter part the slope ξ is $\simeq 0.5$ and it is clear that in observational (N–T) diagrams we will not be able to distinguish such a case from the evolution proceeding strictly along the QSS-branch. Therefore we include the case $\tau = 300$ s in the

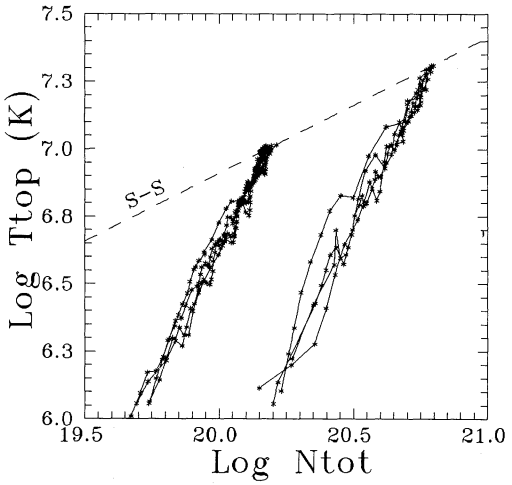

Fig. 8. In this figure, the top plasma temperature is plotted against the total number of electrons contained in the coronal portion of the loop ($T > 0.5$ MK) for the SS-OFF models (cf. Fig. 2 for the comparison)

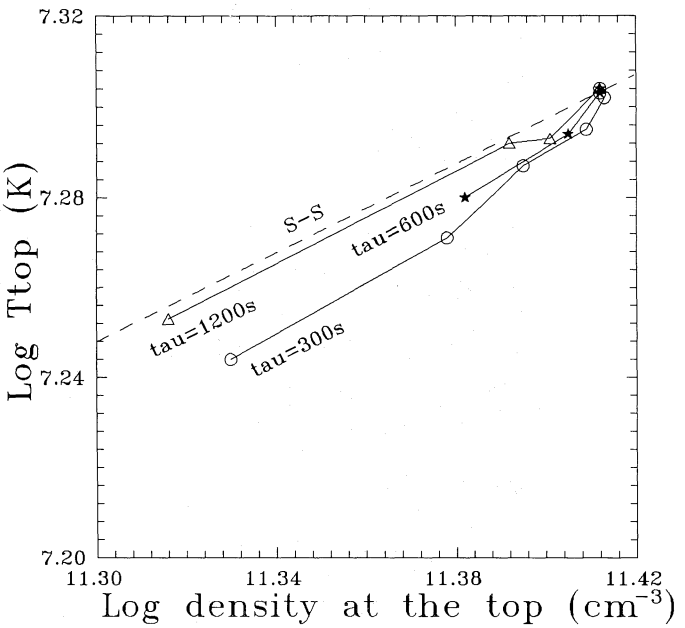

Fig. 9. The N–T diagrams for models of a hot ($T_{top} = 20$ MK) coronal loop ($L = 20$ Mm), initially in steady-state conditions. The heating is decrease exponentially with e-folding decay times of 300, 600 and 1200 s, respectively

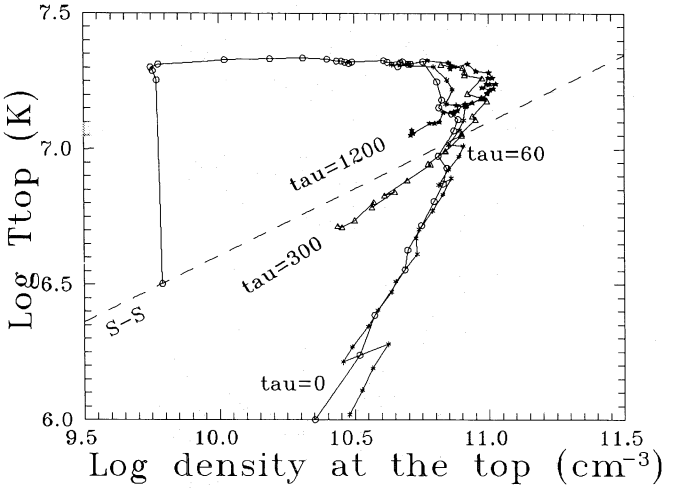

Fig. 10. A density-temperature diagram illustrating the dependence of the **d**-phase slope on the e-folding decay time of the heating rate ($\tau = 60$, 300 and 1200 s cases are shown). The initial constant heating lasted for 180 s

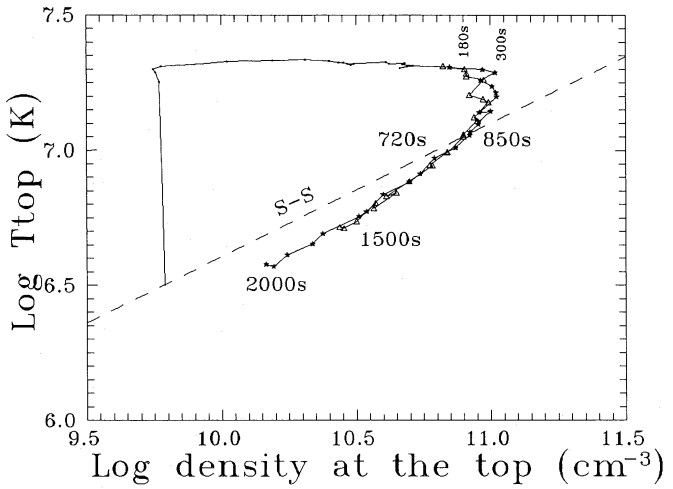

Fig. 12. A comparison of evolutionary paths for models with $\tau = 300$ s and various durations (180 and 300 s) of the initial constant heating

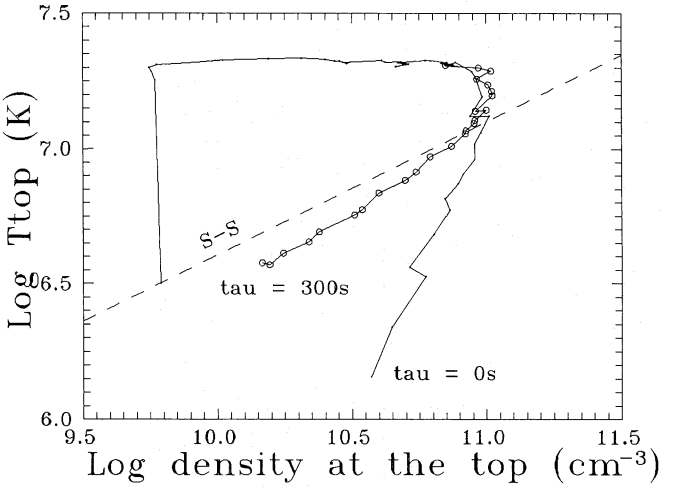

Fig. 11. As in Fig. 10, but here the period of constant heating was 300 s and $\tau = 300$ s

family of QSS-evolution cases as a marginal one. We see that for $\tau = 1200$ s the evolution precedes exactly along the QSS-branch.

(2) Next, we have investigated how the transition of a flare from the **b**-phase to the QSS-phase occurs. To this end, we have calculated the evolution of flare models with the following time-variation of the heating function:

$$E_H(t) = \begin{cases} a = \text{const} & \text{for } 0 < t \leqq \Delta t \\ a \exp(-t/\tau) & \text{for } t > \Delta t\,. \end{cases} \quad (5)$$

We have taken $a = 10$ ergs cm^{-3} s^{-1}, $\Delta t = 180$ s or 300 s and $\tau = 60$ s, 300, or 1200 s.

The results of the calculations are presented in the (N–T) diagrams in Figs. 10, 11, and 12. It is seen from the figures that for a sufficiently slow decay of the heating function ($\tau \geqq 300$ s for the case of $L = 20$ Mm) the evolutionary paths *smoothly* pass from the phase **b** to the QSS evolution. The latter has a slope $\xi \approx 0.5$. Let us note that the heating function decay time of 300 s amounts to about 1.8 of the entropy decay time τ_{th} (cf. the B2 model in Table 1 of Paper I). In the figures we see, moreover, that the QSS-evolution does not run exactly along the S–S line, but parallel to it, at a small distance ($\Delta \log T \simeq 0.1$) from the line. The QSS-branch can run below the S–S line, as well as above it (cf. the evolutionary path for $\tau = 1200$ s in Fig. 12). We consider these small displacements of the QSS-branches relative to the S–S line as being due to the rearrangement of the structure of a cooling loop toward the QSS conditions during the **c**-phase. This effect will be further examined in one of forthcoming papers.

5. Summary and conclusions

The main aim of the present paper was detailed analysis of the flare evolution in (N–T) diagnostic diagram. It has been confirmed that the evolutionary paths in the diagrams are very sensitive to the $E_H(t)$ variations. This confirms, in turn, the high efficiency of our method of analysis of real solar flares (Jakimiec et al. 1986, 1987). The main points of the method are the following:

(1) We construct the empricial (N–T) diagrams using high-quality X-ray observations.

(2) By detailed comparison of the empirical (N–T) diagrams with the calculated ones, we can draw reliable conclusions about the time variations of the thermal energy release, $E_H(t)$, in the investigated solar flares.

Thus, in our method of flare analysis, the (N–T) diagrams are in fact the diagnostic diagrams for the basic physical quantity, the flare energy release $E_H(t)$. At present, it is the most efficient method for diagnosing $E_H(t)$ from flare observations.

In the next paper (Paper III of this series) we will use this method for investigation of many flares which were recorded from the Solar Maximum Mission satellite.

Let us now briefly summarize the main conclusions about the flare evolution in (N–T) diagrams which have been obtained in the present paper:

(I) In the diagnostic diagrams it is easy to distinguish characteristic phases of the flare evoluton which are due to specific changes of the heating function $E_H(t)$, (cf. Figs. 1 and 11).

(II) If $E_H = \text{const}$ in the **b**-phase (flare heating and chromospheric evaporation), the flare evolves along a horizontal line, $T \simeq \text{const}$, (cf. Figs. 1 and 4). The value of the heating function E_H can be estimated from the (N–T) diagrams if we know the loop

semi-length L, ($E_H \approx 1.0\ 10^{-6}\ T^{3.5}\ L^{-2}$, cf. Jakimiec et al. 1986), and the duration of the successive phases **a**, **b**, **c**, ... can be easily read out from the diagrams. If there are some significant variations of the heating function during the **b**-phase, they will be also seen in the (N–T) diagrams (cf. the variation in temperature during **b**-phases in Figs. 6 and 7a).

(III) Very important results have been obtained for the cooling phases of flares. According to our previous suggestions (Jakimiec et al. 1986, 1987) we have two characteristic limiting branches of flare evolution during these phases:

(1) The banch of fast cooling when the flare heating decreases quickly, $\tau \leqq \tau_1(L)$, ($\tau_1 \approx 60$ s for the case of $L = 20$ Mm). The branch has characteristic slope $\xi \simeq 2.0$ in the (N–T) diagrams. This is the case of free of nearly-free evolution of the flaring loop, when the heating decreases so quickly that it does not influence the rate of flare cooling. The rate of flare cooling and the decrease of the density in this case are determined only by the inertia of the processes of heat and plasma outflow from the flaring loop. The calculated models with an abrupt switch-off of the flare heating ($\tau = 0$) represent some idealization of this case.

(2) The QSS-branch of flare evolution, when the heating function is sufficiently slow, $\tau \geqq \tau_2(L)$, where $\tau_2(L)$ is a critical value ($\tau_2 \approx 300$ s in our case). The characteristic slope is $\xi \approx 0.5$. In this case the cooling rate and the plasma outflow are entirely determined by the time evolution of the heating function $E_H(t)$. In the case when a real flare evolves along the QSS-branch, we can also determine the characteristic time τ of the decrease of heating. It can be estimated from the rate of the flare evolution along the QSS-branch, $d(\log T)/dt$.

Moreover, from the above discussion of the limiting cases (1) and (2) it is easy to guess that for the intermediate values of τ, $\tau_1 < \tau < \tau_2$, ξ will be a monotonic function of τ. It will decrease from 2.0 to 0.5 when τ increases from τ_1 to τ_2. Physically these are mixed cases: they are partly controlled by the rate of the heating function decrease and partly by the inertia of the heat and plasma outflow. This functional dependence $\xi(\tau)$ for $\tau_1 < \tau < \tau_2$ will be a subject of detailed investigation in one of the forthcoming papers.

In the next paper (Paper III) all the properties of the flare evolution in the (N–T) diagrams discussed in the present paper, will be used for detailed diagnostics of the time-variations of the energy release, $E_H(t)$, in real flares.

Acknowledgements. This work has been supported by the Polish Academy of Sciences Program CPBP 01.20 (Development and Exploitation of Space Research), and by Agenzia Spaziale Italiana, the Italian National Research Council (CNR) and Ministerio dell'Università e della Ricerca Scientifica e Tecnologica.

References

Fisher G. H., Hawley S. L., 1990, ApJ 357, 243
Jakimiec J., Sylwester B., Sylwester J., Lemen J. R., Mewe R., Bentley R. D., Peres G., Serio S., Schrijver J., 1986, Adv. Space Res. 6, No. 6, 237
Jakimiec J., Sylwester B., Sylwester J., Lemen J. R., Mewe R., Bentley R. D., Peres G., Serio S., Schrijver J., 1987, in: Solar Maximum Analysis. Stepanov V. E., Obridko V. N. (eds.), VNU Science Press, Utrecht, p. 91
Pallavicini R., Peres G., Serio S., Vaiana G., Acton L., Leibacher J., Rosner R., 1983, ApJ 270, 270
Peres G., Rosner R., Serio S., Vaiana G. S., 1982, ApJ 252, 791
Peres G., Serio S., 1984, Mem. Soc. Astron. Ital. 55, 749
Rosner R., Tucker W. H., Vaiana G. S., 1978, ApJ 220, 643
Serio S., Peres G., Vaiana G. S., Golub L., Rosner R., 1981, ApJ 243, 288
Serio S., Reale F., Jakimiec J., Sylwester B., Sylwester J., 1991, A&A 241, 197 (Paper I)
Vernazza J. E., Avrett E. H., Loeser R., 1980, ApJS 45, 619